Available on CMS information server

CMS NOTE-2008/016

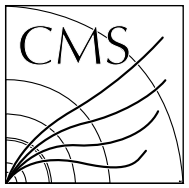

The Compact Muon Solenoid Experiment

CMS Note

Mailing address: CMS CERN, CH-1211 GENEVA 23, Switzerland

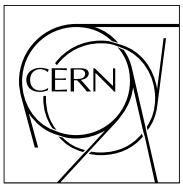

12 March 2008

Measurement of the charge ratio of cosmic muons using CMS data

M. Aldaya, P. Garcia-Abia

Particle Physics Division, CIEMAT, Madrid, Spain

Abstract

This note presents the measurement of the ratio of positive- to negative-charge cosmic muons, performed as a function of the muon momentum, using data collected by the CMS experiment at the *Magnet Test and Cosmic Challenge*. While the magnet test itself is a milestone in the CMS detector construction, not having physics studies among its primary goals, it provides the high quality data –from a large number of cosmic muons– used in this analysis. This is the first measurement of a physical quantity performed by the CMS experiment.

1 Introduction

The *Compact Muon Solenoid* (CMS) [1] is one of the four detectors being installed at the *Large Hadron Collider* (LHC) [2] at CERN (Geneva, Switzerland). The CMS experiment will search for signals of new physics in the high energy frontier, collecting and analyzing a huge amount of data from proton-proton (pp) collisions at a center of mass energy of 14 TeV [3].

The CMS detector surrounds one of the pp interaction points of LHC. A large, four-Tesla, superconducting magnet hosts a high precision tracking system (including a micro-vertex detector), and electromagnetic and hadron calorimeters (ECAL and HCAL, respectively). Outside the magnet, a large muon detector is interleaved with the iron that acts as the return yoke of the magnet. These electronic devices record the signals of the particles crossing the detector, which are then used to measure their energy, momentum and flight direction. Given the high complexity of the detector, it is essential to test and verify all its components at every step of the construction and assembly procedure, in order to ensure the optimal functioning of CMS when LHC delivers the first beams in 2008.

The detector is pre-assembled in a surface hall (SX5) before being lowered to the cavern. A crucial milestone in the construction of CMS is the *Magnet Test and Cosmic Challenge* (MTCC) [4], a major test of a slice of CMS –performed on the surface– devoted to test the detector: magnet, readout electronics, trigger and data acquisition system (DAQ), alignment, calibration and reconstruction algorithms. High energy muons from cosmic rays are used as a particle beam for this test. Physics studies are not among the primary goals of the magnet test, however it provides high quality data –from a large number of cosmic muons– that are used to perform measurements of physical quantities related to cosmic muons.

The *muon charge ratio*, R, is defined as the ratio of the number of positive- to negative-charge cosmic muons. Atmospheric muons stem from cosmic ray showers, produced via interactions of high-energy cosmic-ray particles, entering the upper layers of the atmosphere, with air nuclei: $(\mathrm{p},\, \mathrm{He},\, \ldots,\, \mathrm{Fe}) + \mathrm{A} \rightarrow \mathrm{hadrons}, \mathrm{e}^{\pm}\gamma$, where $(\pi^{\pm},\, \mathrm{K}^{\pm}) \rightarrow \mu^{\pm} + \nu_{\mu}\,(\bar{\nu}_{\mu})$ and $\mu^{\pm} \rightarrow \mathrm{e}^{\pm} + \nu_{\mu}\,(\bar{\nu}_{\mu}) + \nu_{\mathrm{e}}\,(\bar{\nu}_{\mathrm{e}})$. The charge and momentum dependence of R is determined by the meson production cross sections in these high-energy hadronic interactions. As both cosmic rays and air are mainly protons and nuclei, positive meson production is favored, hence more positive muons are expected. Previous measurements from various experiments [5] show the muon charge ratio to be constant up to a momentum scale of about $500\ \mathrm{GeV}/c$. These measurements are used to constrain parameters relevant to low energy hadronic interactions and to better determine the atmospheric neutrino flux.

This note presents the measurement of the muon charge ratio using CMS data, collected at the MTCC, exploiting the capabilities of the drift-tube muon chambers of CMS. The analysis is performed using the standard CMS reconstruction software, as well as data distribution and job submission Grid tools, in a way similar to that designed for the analysis of the data produced in the pp collisions at LHC.

2 Experimental Setup and Data Samples

The MTCC took place in the second half of 2006. Its main goal was to test the CMS detector using cosmic-ray muons, before it was lowered to the experimental cavern. Important parts of this challenge were: testing and commissioning the superconducting magnet (including cooling, power supply and control system), measuring the map of the magnetic field, checking the movement of the detector when the magnetic field is switched on/off, testing the functionality of the muon alignment system and performing a combined test of the sub-detectors available (tracker, ECAL, HCAL and muon system) in a 30° slice of the CMS detector, using as far as possible final readout, data acquisition and trigger systems. There are documents reporting the operational details of the MTCC [4] and a comparison of commissioning results with simulations [6].

The MTCC was split in two distinct phases of data taking. In Phase I, six tracker layers, two ECAL and fifteen HCAL modules, were used. In Phase II, a field mapper replaced the ECAL and tracker detectors. In both phases, the muon system consisted of a reduced setup of the DT (*Drift Tubes*), RPC (*Resistive Plate Chambers*) and CSC (*Cathode Strip Chambers*) detectors: it included sector five in stations ME+1, ME+2, ME+3, in the end-caps, and stations MB1 to MB4 in sector 10 of wheel YB+1 and in sectors 10 and 11 of wheel YB+2, in the barrel region. The MB4 station at the bottom of sector 10 is split in two chambers, which is particularly relevant to the analysis. Figure 1 (left) depicts the experimental setup of the MTCC. A cosmic muon detected in CMS during the MTCC is displayed in figure 1 (right).

Around 25 million "good" events were recorded with at least DT triggers, of which 15 million were at a stable magnetic field above 3.8 T. The data files were transfered from SX5 to a disk pool (CASTOR) at the CERN site (Tier-0) and processed quasi-online. Both raw and processed data were distributed to several Tier-1 centers (Fermilab and

PIC, for example) using PhEDEx [7] and subsequently transfered to various Tier-2 centers (like CIEMAT). Skimming jobs were submitted to LCG (the LHC Computing Grid), using the standard CMS job submission tool [8], and the output was collected at Tier-3 centers where the final analysis was performed.

One important milestone of the MTCC was to establish the proper functioning of the data acquisition system using different trigger configurations. This yielded a large amount of data collected in quite different working conditions of the detector. In order to guarantee the uniformity of the muon sample, only events triggered by the DTs are accepted for the analysis. Furthermore, the analysis is performed with the information from the DT muon chambers alone, hence nearly vertical muons are selected. Table 1 details the MTCC runs used in the analysis, along with their magnetic field, trigger configuration, numbers of events and the fraction of events triggered by the DTs relative to the total number of triggered events.

Table 1: Run numbers, magnetic field (values in Tesla), numbers of events and fraction of events triggered by the DTs relative to the global trigger rate, for the MTCC runs used in the analysis. All runs are from MTCC phase II, except run 2377.

Run	B (T)	Trigger conditions	Events	DT trigger rate
2377	3.67	DT (MB2, MB3), CSC (first 160703 events); CSC, DT, RPC (from event 160704)	613 174	20 %
4045	3.8	DT (MB1, MB2, MB3) OR CSC	3 110 980	32 %
4406	4	DT (MB2, MB3) OR CSC	1 825 273	23 %
4407	4	DT (MB2, MB3) OR CSC	1 665 440	23 %
4409	4	DT (MB2, MB3) OR CSC	2 563 020	23 %
3809	0	any two DT chambers coincidence	611 407	99 %

The CMS detector is built to detect and measure the properties of particles produced in a central vertex from LHC-delivered pp collisions. The flight direction of cosmic-ray muons and the randomness of their arrival time make these particles behave quite differently, CMS wise, from those coming from the nominal interaction vertex, requiring special trigger configurations, reconstruction software and calibration procedures.

The events are reconstructed using the standard reconstruction software [9] of the CMS experiment. The so-called *Standalone muon reconstruction* was adapted for dealing with the specific spatial configurations of cosmic muons [10]. The measured muon momentum and angles are calculated with respect to the entry point of the muon in the innermost DT station (MB1). The reconstruction procedure uses special DT calibration constants, in order to have a common reference for trigger synchronization [11]. This special calibration is crucial to account for the random arrival time of cosmic muons. Alignment corrections [12], calculated from survey data [13], are applied to the measured hits (signals in the DTs) before the track reconstruction. These corrections take into account the relative alignment of the superlayers within a chamber (so called internal alignment), measured in an optical bench at CERN. Alignment, being the main source of systematic uncertainty in this analysis, in particular for particles with a momentum in excess of about 100 GeV/c, deserves a more detailed study (section 4).

While this analysis is mostly data driven, simulated samples of cosmic muons that reproduce the MTCC setup exist [6] and are used for cross checks and to extract some minor corrections (section 4). Two samples of one-million events are generated with the CMSCGEN program [6], one with zero magnetic field and the other with $B = 4$ T. After full simulation, digitization, reconstruction and trigger simulation, only about 1% of these simulated events fulfill the MTCC acceptance and trigger conditions.

In order to select events containing well-reconstructed muons, the following preselection criteria are required:

1. at least 6 hits in both ϕ superlayers of the MB2 and MB3 stations, for both wheels YB+1 and YB+2,
2. at least one reconstructed muon track in the DTs,
3. all the hits of the muon track must be in sector 10,
4. and the point of closest approach of the muon track to the nominal CMS center must be inside the magnet volume, which is a special feature of the *CosmicMuonReco* code [10].

The numbers of events surviving these criteria are listed in table 2 (left), together with the relative efficiencies of the cuts (relative to the numbers of events triggered by the DTs), for the runs used in the analysis. Figure 2

displays the distributions of the momentum of the muon tracks, their azimuthal (ϕ) and polar (θ) angles –measured at the innermost station–, and the number of reconstructed hits per track, for preselected events. The global CMS coordinate system is used, in which the z axis goes along the beam-line, that is, $\phi = -90^\circ$ and $\theta = 90^\circ$ for vertical muons.

Table 2: Numbers of events and relative efficiencies of the cuts, per run and for all runs together, after preselection (left) and selection (right) criteria are applied. The fractions of quadruplets in the sample, denoted by Q/(Q+T), are also listed for the selected samples (right). The definitions of the relative efficiencies are detailed in the text.

Preselection		
Run	Events	Relative efficiency
2377	40 650	33 %
4045	280 165	28 %
4406	147 471	35 %
4407	135 209	35 %
4409	207 985	35 %
Total	811 480	29 %

Selection			
Run	Events	Relative efficiency	Q/(Q+T)
2377	16 908	42 %	54.9 %
4045	123 916	44 %	78.5 %
4406	59 227	40 %	79.2 %
4407	54 028	40 %	79.2 %
4409	83 036	40 %	78.9 %
Total	337 115	42 %	77.6 %

The agreement among data from the different runs is excellent, in particular for those with the same trigger conditions. A slight difference in the ϕ distribution is observed for run 4045, which is due to its different trigger configuration. The run 2377 serves as a good example of the difficulties found in the analysis of the MTCC data: the trigger configuration changed with time, there were problems in wheel YB+2 and instabilities in the global DAQ. All this caused a lower efficiency and some distortions visible in the distributions of figure 2.

Good agreement of the simulations with the data is also observed, after scaling the momentum of the simulated events by 1.25 to better describe the data. Some disagreement is visible at very low momentum, due to the cut $p > 7$ GeV/c for simulated events, and in the number of hits per track, as noise and dead cells are not included in the simulations.

3 Analysis and Event Selection

The analysis strategy is selecting a sample of high quality muons, obtaining the momentum spectra as function of the muon charge and calculating the charge ratio as a function of the momentum, $R(p)$. Given the experimental setup, the mean value of the charge ratio and its uncertainty are expected to be dominated by the measurements at low momentum, below $p \simeq 100$ GeV/c.

In order to make the analysis mostly data driven, that is, to avoid its dependence on detailed simulation studies and corrections, some important considerations are taken into account. Muons leaving signals in either two (*doublets*), three (*triplets*) or four (*quadruplets*) DT stations, have different numbers of hits, yielding different momentum resolutions. The μ^+ and μ^- populations must have similar momentum resolution, therefore the analysis is done in a way not to favor any particular charge and quality (at the same time), which is achieved by requiring good muons to be either triplets (leaving signals in MB1, MB2 and MB3) or quadruplets in the muon system. This is particularly important at high momentum, $p \gtrsim 100$ GeV/c, where momentum resolution worsens significantly. The comparison of the individual results for triplets and quadruplets helps in establishing possible biases due to miscalibration and misalignment.

Due to the magnetic field, unlike-sign charged particles bend in opposite directions in the R-ϕ plane (transverse to the beam axis), populating different regions of the detector. This, together with the trigger configuration (MB2+MB3), introduces a bias in the relative detection efficiency of μ^+ and μ^-. The trigger-induced asymmetry is visible, for example, in the distribution of hits in the detector, shown in figure 3 (left) for run 3809. This run was collected at $B = 0$, the observed effect is therefore independent of the muon charge. In order to avoid such bias in the relative efficiency of μ^+ and μ^-, the fiducial geometric acceptance of the detector is constrained to be left-right symmetric with respect to the axial (vertical) axis of the detector in the R-ϕ plane. In addition, the detector efficiency within the fiducial volume must also be left-right symmetric in R-ϕ (though not necessary flat). The graph in figure 3 (right) helps understanding the influence of the geometric acceptance in the relative efficiency for μ^+ and μ^- with the same momentum, entering the detector in symmetric points, and with the same angle, with respect to the vertical axis.

A high-quality sample of *golden* muons that avoids biasing the relative acceptance of positive and negative muons

is selected as follows. All reconstructed muon tracks are required to have a momentum above 3 GeV/c and must have hits at least in three chambers (one of them being MB1), which ensures a precise measurement of momentum and angles. Only tracks going through a single wheel are considered: by discarding the small amount of wheel-crossing tracks, non-vertical muons are rejected and, more important, the relative alignment between wheels becomes irrelevant.

The left-right symmetric fiducial geometry is imposed by requiring all the track hits to have a global X coordinate inside the region $[-a, a]$, where a, in cm, equals 60, 90, 120 and 185 for MB1, MB2, MB3 and MB4, respectively (figure 3 (right)). The MB2+MB3 trigger efficiency is very high in this region (figure 3 (left)) and the muons selected in this geometry are close to vertical, with an incidence angle lower than 40°. Other symmetric regions are considered in the analysis ($a = 60$ cm for all the chambers) in order to study potential systematic effects due to detector performance in the fiducial geometry. The distributions of hits for selected events of run 4406, collected at $B = 4$ T, are displayed in figure 4, separately for positive and negative muons in the fiducial volume of wheel YB+1. The two graphs are mirror images of each other (due to the different muon charges), reflecting the left-right symmetry of the fiducial geometry in the R-ϕ plane.

The numbers of events and relative efficiencies of the cuts (relative to the numbers of preselected events), after the selection criteria above are applied, are listed for each run in table 2 (right), along with the fractions of quadruplets in the selected samples. The distributions of the transverse momentum of the muon tracks, their azimuthal and polar angles, and of the number of reconstructed hits per track, are shown in figure 5 for the selected events. The selection of golden events improves the quality of the distributions, making the differences among runs very small. Simulation reasonably agrees with data, despite its relative lack of realism: detector noise, dead cells and cell inefficiencies are not in the simulation, and the trigger is modeled only approximately. The ratio of selected to preselected events is consistent among runs, both for μ^+ and μ^-.

Quality control of detector performance

Non-uniformities of the detector –hot spots, dead or inefficient regions– would impact differently the detection efficiency of unlike-sign charged particles, introducing a bias in the measurement of the charge ratio. Both the uniformity of the detector and the left-right symmetry of its efficiency within the fiducial volume are verified at different levels of the selection procedure. This is done using a control data sample, collected at $B = 0$, which is therefore not used in the analysis.

Almost vertical straight muons are selected requiring tracks with an incidence angle below 30°. In addition, a lower cut on the track momentum is imposed at 15 GeV/c, in order to reject tracks significantly bent by multiple scattering in the magnet yoke. The selected muons uniformly illuminate the fiducial volume of the muon detector. The symmetric behavior of the detector –in terms of cell occupancy– is assessed, in a layer-by-layer basis, using the distribution of hits as a function of the global X coordinate in two halves of the selected region, folding the $-X$ side onto the $+X$ one, in the $[0, a]$ range, a as defined above. This is done for all the 64 R-ϕ layers of the muon detector. As an example, figure 6 shows these distributions for one particular superlayer (adding up four layers, for clarity). The dead cells (less than 1% of the total) have a negligible effect in the track reconstruction.

4 Results

The measurement of the muon charge ratio, R, is computed as the ratio of the p spectrum of positive muons to that of negative muons, as a function of the reconstructed muon momentum (p),

$$R(p) = \frac{N_{\mu^+}(p)}{N_{\mu^-}(p)}\,.$$

The momentum spectrum rapidly decays for increasing p values, hence the size of the p bins is chosen so as to have a minimum number of events to allow a proper calculation of that ratio. The bin edges, in GeV/c, are 0, 5, 10, 15, 30, 60, 100, 200 and 1000 (infinity, indeed). In the charge ratio graphs, the average momentum in each bin is taken as the p value, rather than the center of the bin.

The measured muon charge ratio and its statistical uncertainty are displayed in figure 7, for quadruplets and triplets, for the individual runs analyzed. The charge ratio is mostly momentum independent, up to $p \simeq 200$ GeV/c. Triplets, not crossing the MB4 chamber, are not sensitive to misalignment effects in the two halves of that muon station, unlike quadruplets. The results obtained for triplets and quadruplets are mutually consistent and the deviations observed among different runs are consistent with statistical fluctuations, both giving confidence in the result.

The combined results for all the runs collected at $B = 4$ T are shown in figure 8 (left) for quadruplets, triplets and their combination. The agreement is excellent up to 200 GeV/c. The discrepancy in the last momentum bin is attributed to alignment effects which, being significantly different for triplets and quadruplets, are most important at high momentum. As a cross check, similar results are depicted in figure 8 (right) for run 3809, collected at $B = 0$. In this case, for which there is no valid information about the muon momentum and charge, the results are consistent with one, supporting the robustness of the analysis even in odd conditions.

Potential sources of systematic uncertainty affecting the measurement of the charge ratio are the accuracy of the magnetic field, the detector performance in the fiducial region, the alignment of the muon detector and the charge confusion. Detailed studies confirm the stability of the result with respect to variations of the magnetic field and the fiducial geometry.

Both, the relative alignment of the muon chambers and the internal alignment of the superlayers within a chamber, play a crucial role in the analysis. Deviations from an ideally aligned detector yield systematic shifts in the measured muon momentum and, at high momentum, even swap the muon charge. Most important, these deviations are anti-symmetric for μ^+ and μ^-, having a potentially large impact in the measurement of the charge ratio, in particular for high momentum muons.

The alignment constants used to correct the hit positions prior to track reconstruction are extracted from survey data [12, 13] and from the measurements of the relative (internal) alignment of the superlayers within a chamber. The impact of the alignment on the measurement is evident in figure 9, where the charge ratio is displayed in two scenarios: aligned and not-aligned. The charge ratio measurement averaged over the two wheels (whole sample), presents a highly unstructured shape in the case misalignment is not corrected for, which is in contrast with the flat shape for the aligned scenario. In both cases, aligned and not-aligned, there is a systematic difference in the charge ratio calculated in the two wheels separately, more evident at high momentum.

The systematic error due to misalignment is estimated by varying the alignment constants within their errors, and quantifying the variation induced in the charge ratio. These errors are much smaller (around 4 to 8 times) than the correction itself, which reflects the importance of the alignment correction. The systematic uncertainty from misalignment is displayed in figure 10, as a function of the measured muon momentum. The difference in the charge ratio measured in the two wheels separately, also depicted in figure 10, is consistent with this uncertainty.

Due to the detector momentum resolution, the probability for the correct assignment of the muon charge is not 100%, making the measured charge ratio deviate from the true value. Assuming the muon charge misidentification probability (charge confusion), $C(p)$, is charge symmetric, the observed numbers of μ^+ and μ^- ($N_{\mu^\pm}$) are functions of the true numbers of μ^+ and μ^- ($N^\circ_{\mu^\pm}$),

$$N_{\mu^\pm} = (1 - C)\, N^\circ_{\mu^\pm} + C\, N^\circ_{\mu^\mp},$$

where the p dependence is not made explicit for clarity. The *true* muon charge ratio, R°, expressed in terms of the observed quantity, is

$$R^\circ = \frac{R - C\,(1 + R)}{1 - C\,(1 + R)}.$$

A linear parameterization of $C(p)$ is made, as a function of p, using simulated events that pass the selection cuts (figure 11 (left)). This correction is slightly larger for triplets than for quadruplets. The value of C is less than 5% for low momentum tracks, below $p \simeq 100$ GeV/c, and increases significantly (up to 40%) for high momentum muons. While the charge confusion in the simulations is not expected to accurately reproduce that of data, the large errors in the parameters of $C(p)$, dominated by the small number of simulated events, exceed the expected accuracy. Hence, these errors are considered a systematic uncertainty in the determination of the charge ratio and are depicted in figure 10. The effect of the charge confusion correction in the measurement of the charge ratio is displayed in figure 11 (right).

In order to compare the CMS results with the measurements from other experiments, the charge ratio is expressed in terms of the muon momentum *before entering CMS*, referred to as the *true* muon momentum. For that, a mapping of the measured into the true muon momentum is performed using simulated events. The overall effect of this correction is an almost constant momentum increase of about 7 GeV/c, having a negligible impact in the charge ratio measurement.

The measurement of the charge ratio using CMS data as a function of the true muon momentum, along with the statistical and systematic uncertainties, is depicted in figure 12 and the corresponding values are listed in table 3. Given the experimental accuracy, the charge ratio is consistent with being independent of the muon

Table 3: Numbers of positive and negative muons selected ($N_{\mu^\pm}$), measurement of the charge ratio (R) and measurement of the *true* charge ratio (R°), using CMS data, in various bins of the true muon momentum (p), along with the statistical (ΔR°_{stat}) and systematic (ΔR°_{syst}) uncertainties.

$\langle p \rangle$	N_{μ^+}	N_{μ^-}	R	R°	ΔR°_{stat}	ΔR°_{syst}
12.1	25 050	19 283	1.299	1.302	0.012	0.010
13.8	57 404	45 298	1.267	1.271	0.008	0.019
16.3	32 386	25 772	1.257	1.263	0.010	0.021
20.7	40 444	32 253	1.254	1.267	0.009	0.028
30.9	20 685	16 284	1.270	1.294	0.013	0.043
48.3	6 790	5 567	1.220	1.268	0.022	0.056
78.3	3 685	3 058	1.205	1.315	0.029	0.107
200.0	1 638	1 518	1.079	1.219	0.038	0.273

momentum in the range of study. Under this assumption, the mean value of the charge ratio, integrated over the muon momentum, is

$$\begin{aligned} \langle R^\circ \rangle &= 1.282 \pm 0.008 \\ &= 1.282 \pm 0.004\,(\text{stat.}) \pm 0.007\,(\text{syst.}) \end{aligned}$$

This value is obtained combining the charge ratio measurement at the various momentum bins, taking into account the statistical and systematic uncertainties and their correlations, using the method of reference [14]. The statistical component of the error, 0.004, is defined as the error obtained when all the systematic uncertainties and their correlations are set to zero. The systematic component, 0.007, is the quadratic difference of the total error and the statistical component. The mean value and its uncertainties are dominated by the measurements at low momentum, below $p \simeq 100$ GeV/c, those at high p being largely dominated by the systematic uncertainty (figure 10). This result nicely compares to those from the most precise experiments [5].

5 Conclusions

We have measured the ratio of positive- to negative-charge cosmic muons, as a function of the muon momentum, using data collected by the CMS experiment at the *Magnet Test and Cosmic Challenge* (MTCC). The analysis has been performed in an environment, CMS and Grid wise, similar to that designed for the analysis of the data coming from pp collisions at LHC, using standard CMS reconstruction software, data distribution and job submission tools. Thanks to this analysis, we have unraveled important issues concerning both the alignment constants of the muon detector and the reconstruction code of CMS. While physics studies were not among the goals of the magnet test, we have succeeded to obtain a result of good quality, which is in agreement with previous measurements within the experimental uncertainties. This is the first measurement of a physical quantity performed by the CMS experiment.

Acknowledgments

We wish to express our gratitude to the CMS colleagues who have set up and run the detector during the MTCC. Especial thanks to P. Biallass, A. Calderón, A. Delgado Peris, M.C. Fouz, J.M. Hernández, K. Hoepfner, P. Ladrón de Guevara, C. Liu, P. Martínez Ruiz del Árbol, A. Meneguzzo and J. Rodríguez Calonge, for technical support and useful discussions. We apologize for those we may have missed.

References

[1] CMS Collaboration, *The CMS experiment at the CERN LHC*, submitted to Jour. Inst. (2007).

[2] LHC: we are not aware of a publication that can be used as a reference for LHC. At least, we mention here the web page of the project, as we consider it sufficiently relevant: *http://cern.ch/lhc/*.

[3] CMS Collaboration, *CMS Physics Technical Design Report, Volume II: Physics Performance*, J. Phys. G: Nucl. Part. Phys. 34 (2007) 995-1579.

[4] CMS Collaboration, *The CMS Magnet Test and Cosmic Challenge (MTCC Phase I and II) Operational Experience and Lessons Learnt*, CMS-NOTE 2007/005.

[5] T. Hebbeker, C. Timmermans, Astropart. Phys. 18 (2002) 107-127;
J.M. Baxendale, C.J. Hume, M.G. Thompson, J. Phys. G 1 (1975) 781-788;
B.C. Rastin, J. Phys. G 10 (1984) 1629-1638;
P. Achard *et al.*, L3 Collaboration, Phys. Lett. B 598 (2004) 15-32.

[6] P. Biallass, T. Hebbeker, K. Hoepfner, *Simulation of Cosmic Muons and Comparison with Data from the Cosmic Challenge using Drift Tube Chambers*, CMS-NOTE 2007/024.

[7] PhEDEx, *Physics Experimental Data Export*, *http://cern.ch/cms-project-phedex/*.

[8] CRAB, *CMS Remote Analysis Builder*, *http://cmsdoc.cern.ch/cms/ccs/wm/www/Crab/*.

[9] Version CMSSW_1_1_1 is used. There is not a publication specific to CMSSW. More information can be found in the web pages:
https://twiki.cern.ch/twiki/bin/view/CMS/WorkBook and *https://twiki.cern.ch/twiki/bin/view/CMS/SWGuide*.

[10] C. Liu, N. Neumeister, *Reconstruction of Cosmic and Beam-Halo Muons*, CMS-NOTE 2008/001.

[11] A.T. Meneguzzo *et al.*, *Method for the Measure of the Time of the Track Passage and of the Drift Velocity in the Drift Tube Chambers of CMS*, CMS NOTE in preparation.

[12] A. Calderón *et al.*, *Muon System alignment with tracks*, CMS-NOTE 2006/016;
A. Calderón *et al.*, *Link Alignment System MTCC Results*, CMS-IN 2007/050.

[13] J.F. Fuchs, R. Goudard and J.D. Maillefaud, *CMS-SUMMARY. YBs and YEs Position w.r.t. YB0 in SX5*, CMS-SG-UR-0490 (2006).

[14] L. Lyons, D. Gibaut, and P. Clifford, *How to combine correlated estimates of a single physical quantity*, Nucl. Instrum. Meth. A 270 (1988) 110;
A. Valassi, *Combining correlated measurements of several different physical quantities*, Nucl. Instrum. Meth. A 500 (2003) 391.

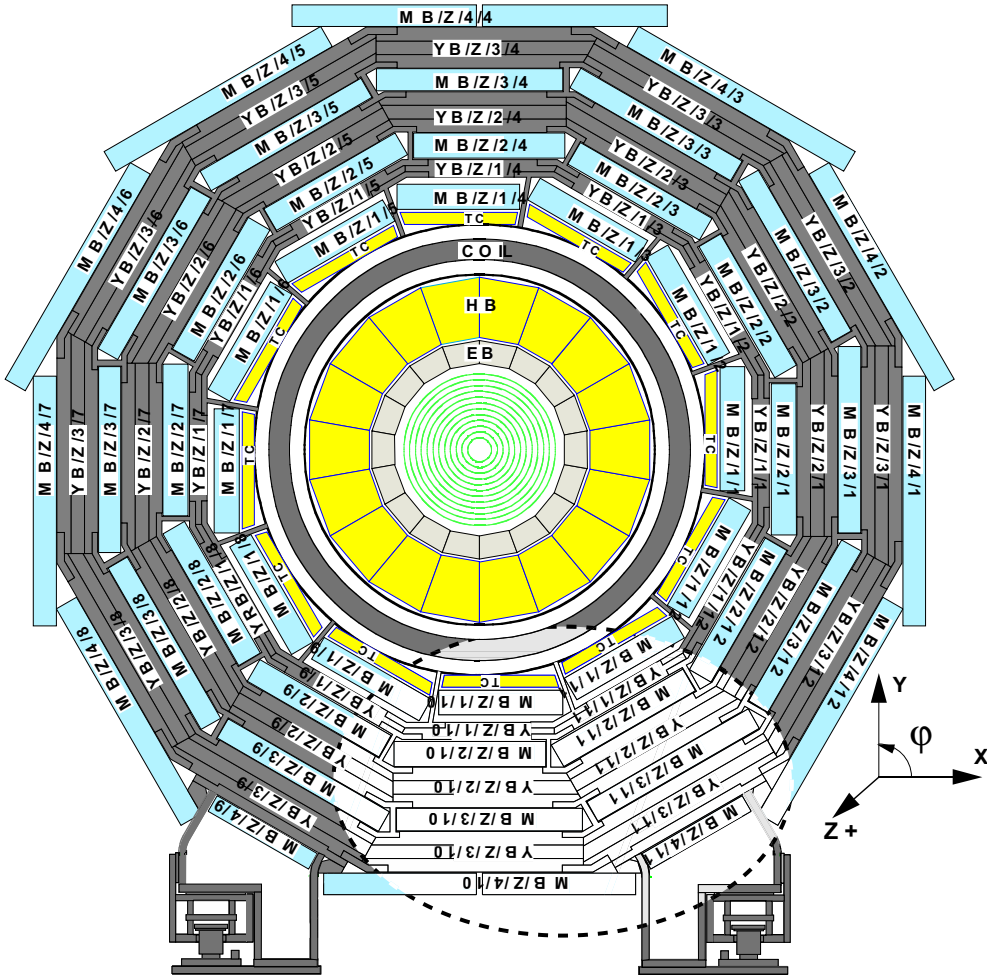

Barrel wheels YB+2 (S10, S11) and YB+1 (S10)

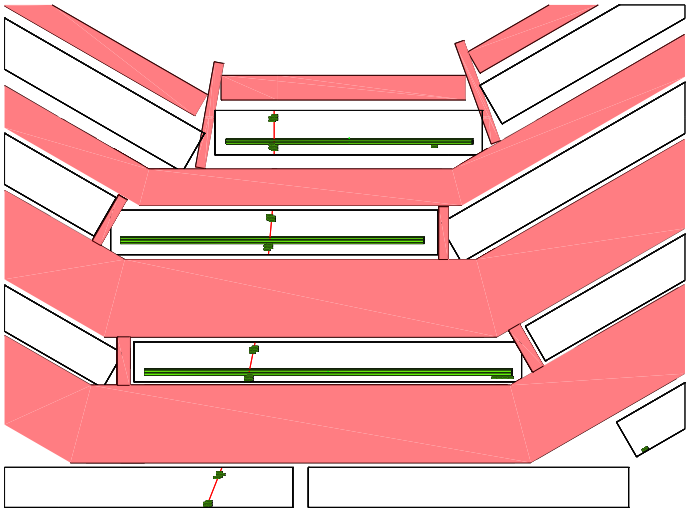

Figure 1: (Top) Transverse, R-ϕ, view of the experimental setup of the MTCC. The slice used in the test, in lighter color, is enclosed in an ellipse-shaped dashed line. (Bottom) A cosmic muon observed with the CMS detector during the MTCC. The green dots and straight lines indicate the hits in the muon system, the thin red lines showing the reconstructed muon track.

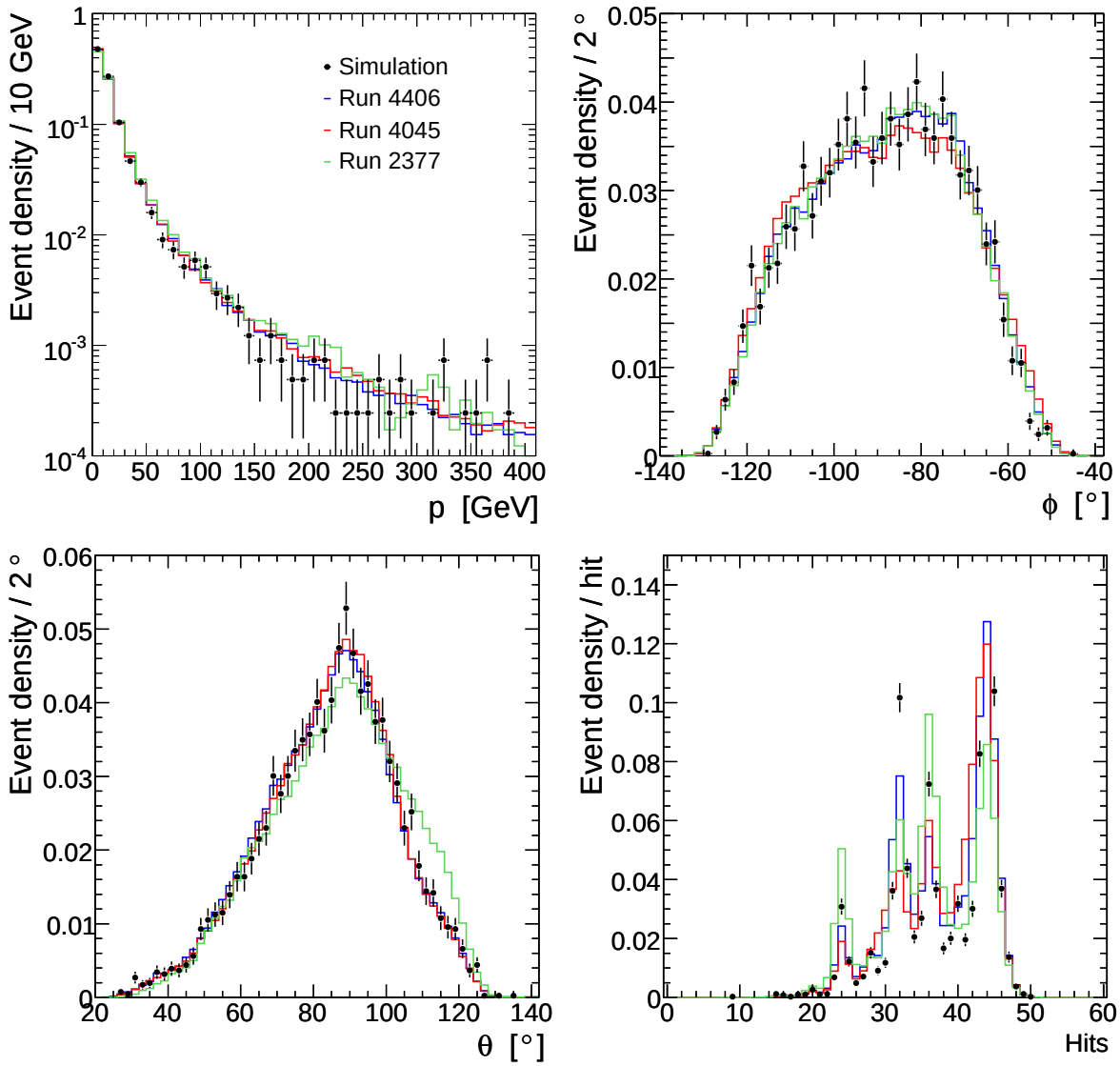

Figure 2: Normalized distributions of the momentum of the muon tracks (upper left), their azimuthal (upper right) and polar angles (lower left), measured at the innermost station, and the number of reconstructed hits per track (lower right), for preselected events. The colored lines correspond to data from different runs and dots with error bars to the simulated events. This unusual choice is due to the tiny size of the statistical errors for the data histograms, as compared to the simulated events.

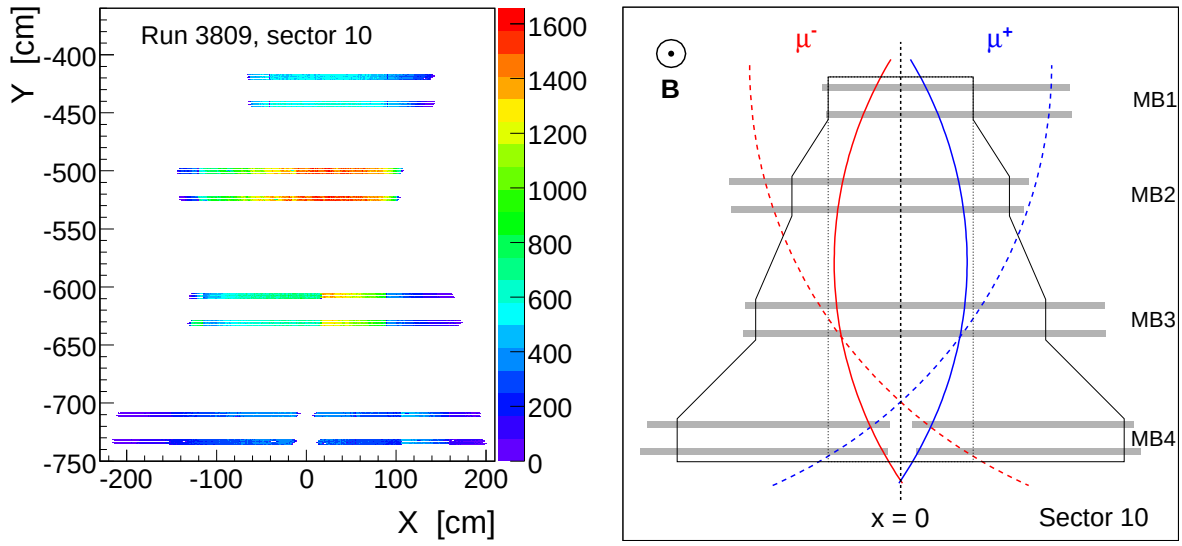

Figure 3: (Left) Distribution of hits in global XY coordinates for run 3809, collected at $B = 0$. The non-uniform cell occupancy, due to the trigger configuration, is evident before symmetrizing the fiducial volume. (Right) Definition of the left-right symmetric fiducial geometry (black solid polygonal line) in the muon system. The dashed lines depict two muon tracks with the same momentum crossing sector 10, the negative one satisfying the MB2+MB3 trigger condition and the positive one failing it. The solid curves represent two muons with the same p in the fiducial geometry, both of them passing the golden muon selection criteria.

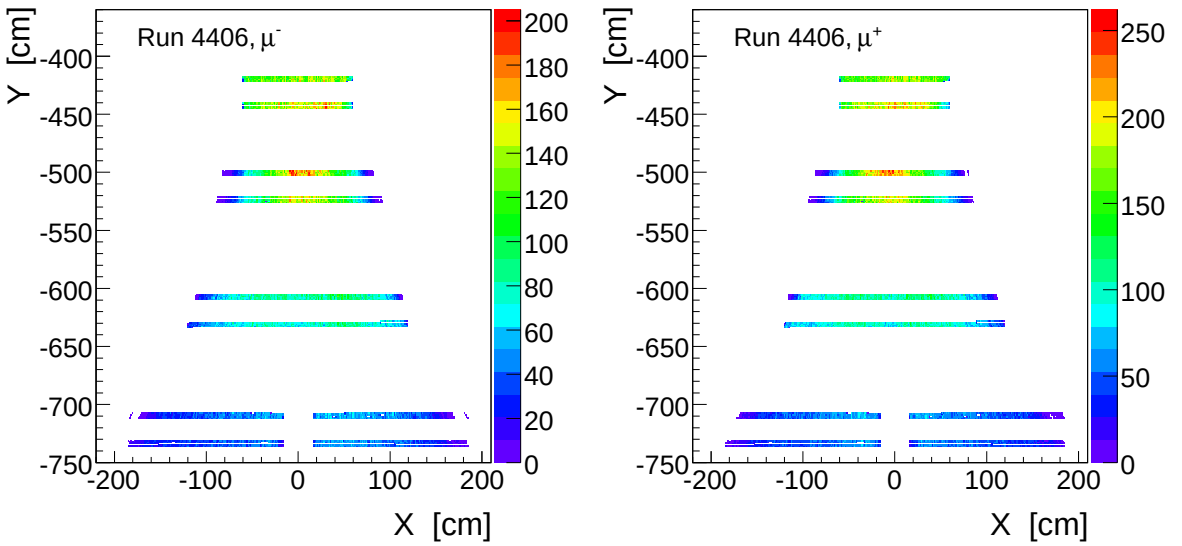

Figure 4: Distribution of hits in global XY coordinates, for (left) negative and (right) positive muons of run 4406 ($B = 4$T) in wheel YB+1, after selection cuts are applied.

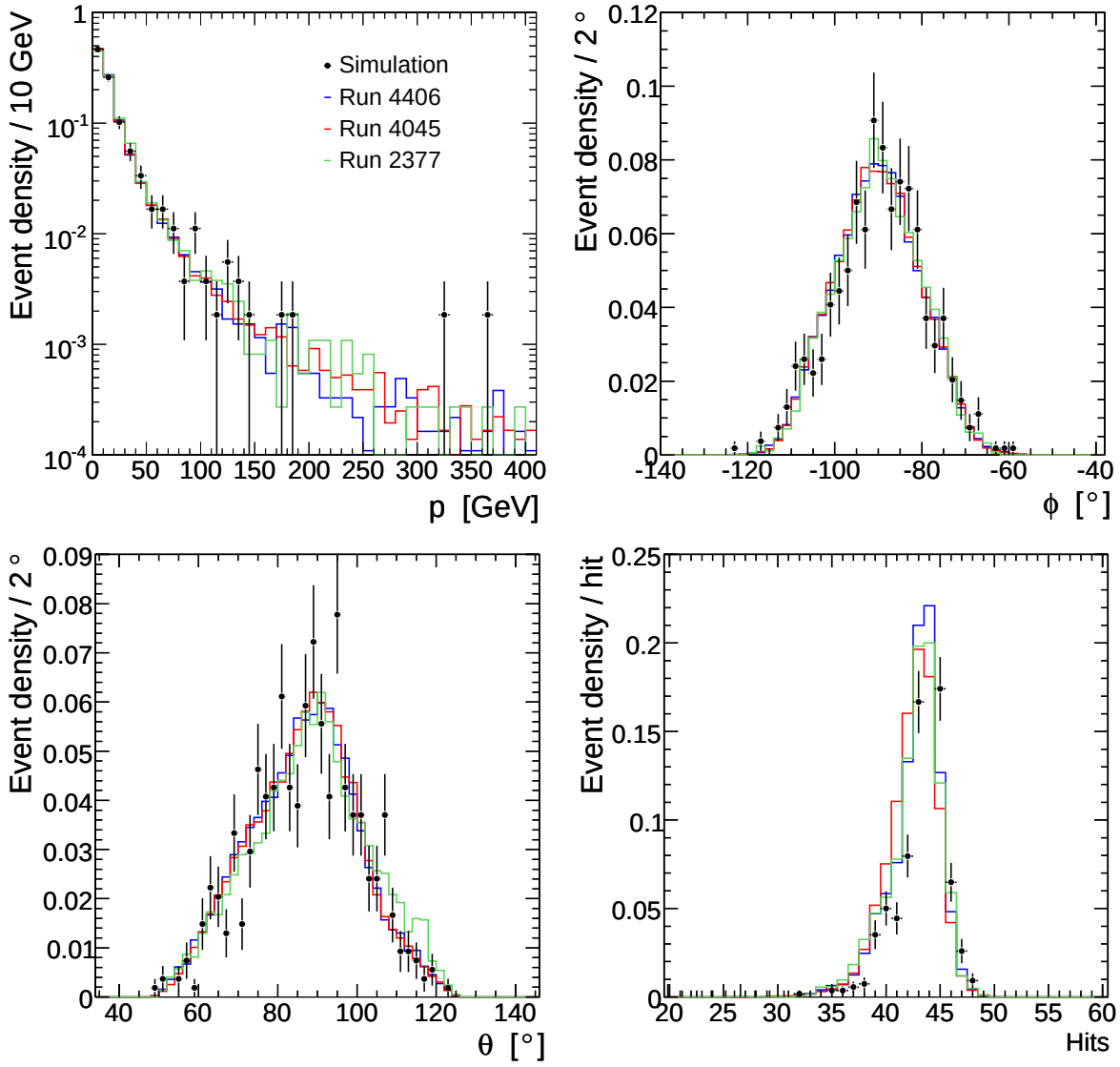

Figure 5: Normalized distributions of the momentum of the muon tracks (upper left), their azimuthal (upper right) and polar angles (lower left), and the number of reconstructed hits per track (lower right), for quadruplet muons in the selected sample. The colored lines correspond to data from different runs and dots with error bars to the simulated events.

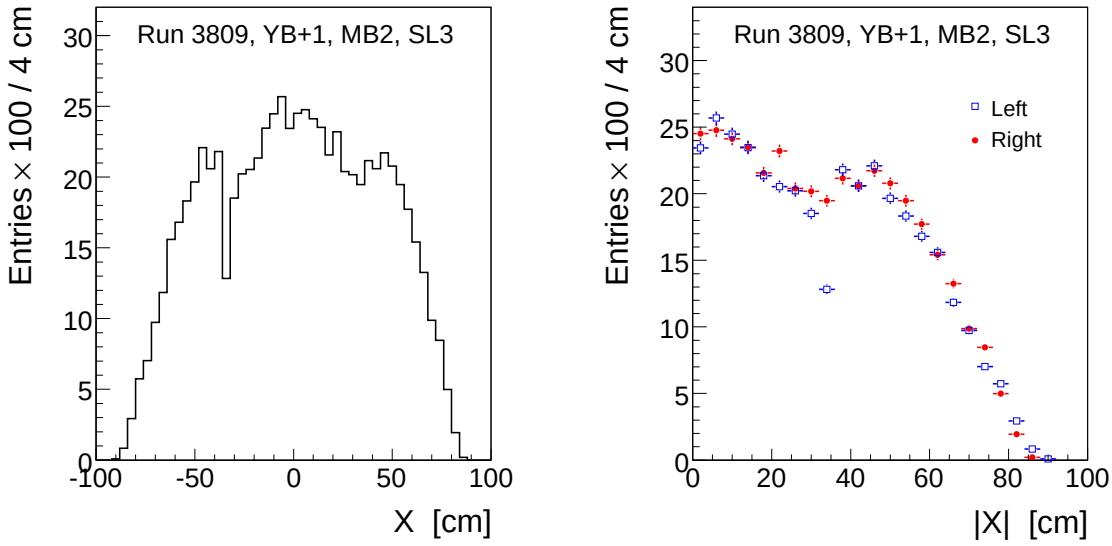

Figure 6: (Left) Distribution of hits in the fiducial geometry of the R-ϕ superlayer 3, chamber MB2, wheel YB+1, as a function of the global X coordinate. (Right) Comparison of the left (blue) and right (red) sides of the hit distribution in that superlayer, as a function of the absolute value of X. The data of the distributions are from run 3809, taken at $B = 0$. The few dead cells around $X \simeq -35$ cm have a negligible effect in the track reconstruction.

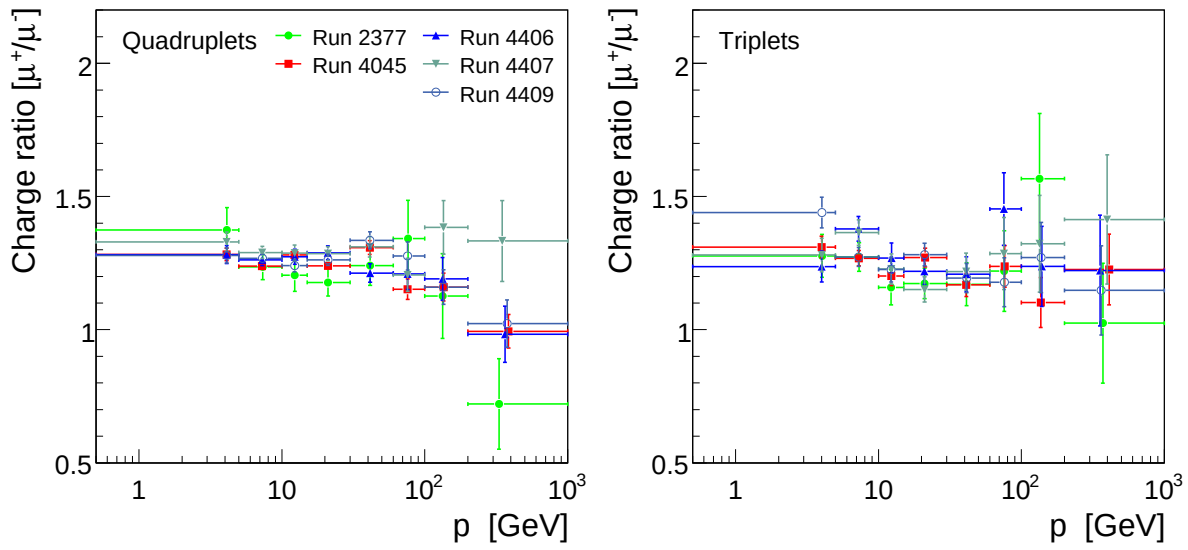

Figure 7: Measured muon charge ratio, as a function of the reconstructed muon momentum, for the individual runs for quadruplets (left) and triplets (right). The p values of the data points represent the average momentum in each bin, for each run separately. The error bars indicate the statistical error.

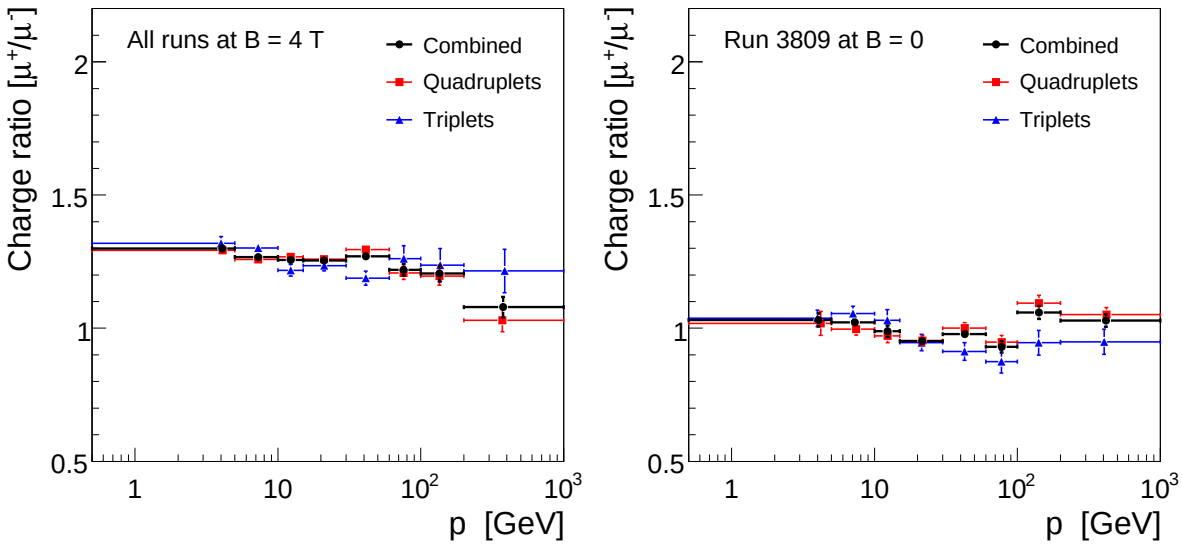

Figure 8: (Left) Measured muon charge ratio, as a function of the reconstructed muon momentum, for all the runs combined, for quadruplets (red), triplets (blue) and their combination (black). (Right) Similar graphs (same color convention), for events from run 3809, collected at $B = 0$, for which there is no valid information about the muon momentum and charge. The error bars represent the statistical error.

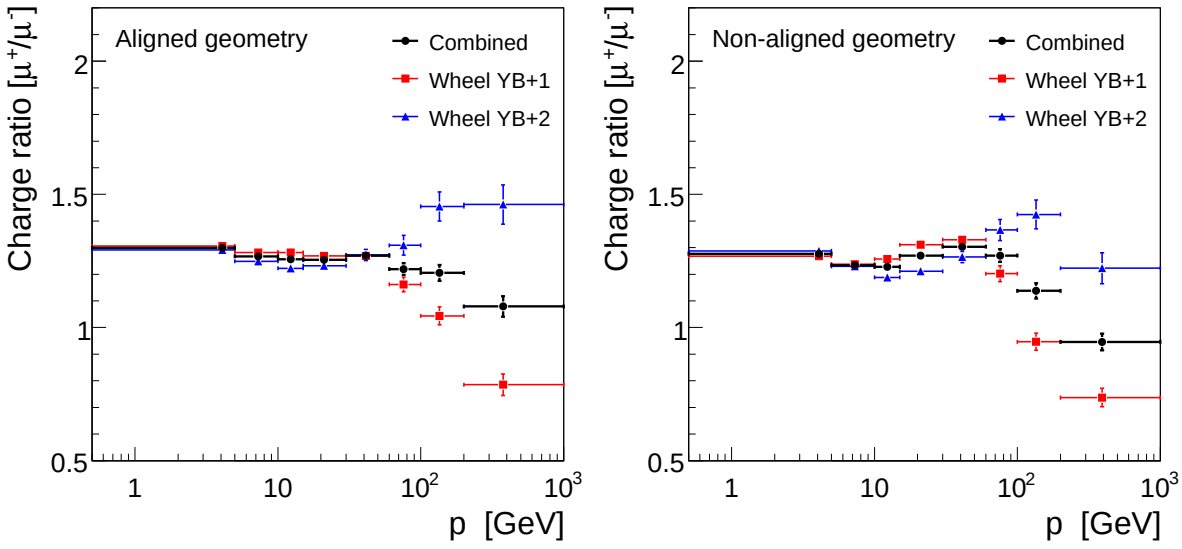

Figure 9: Charge ratio, as a function of the measured muon momentum, with (left) and without (right) the alignment correction, in the two wheels (red and blue dots) and their average value (black) for all the runs combined. The error bars denote the statistical error.

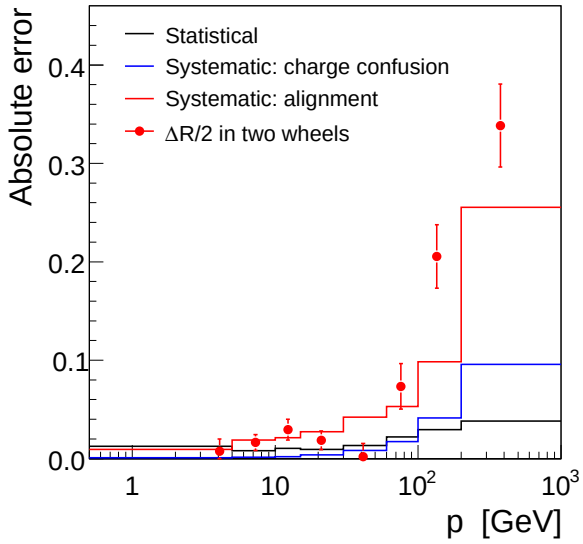

Figure 10: Statistical error on the charge ratio measurement, compared to the individual contributions to the total systematic uncertainty, expressed as a function of the measured muon momentum. For comparison, the semi-difference of the charge ratio measured in the two wheels, YB+1 and YB+2, is also shown as the red dots with error bars.

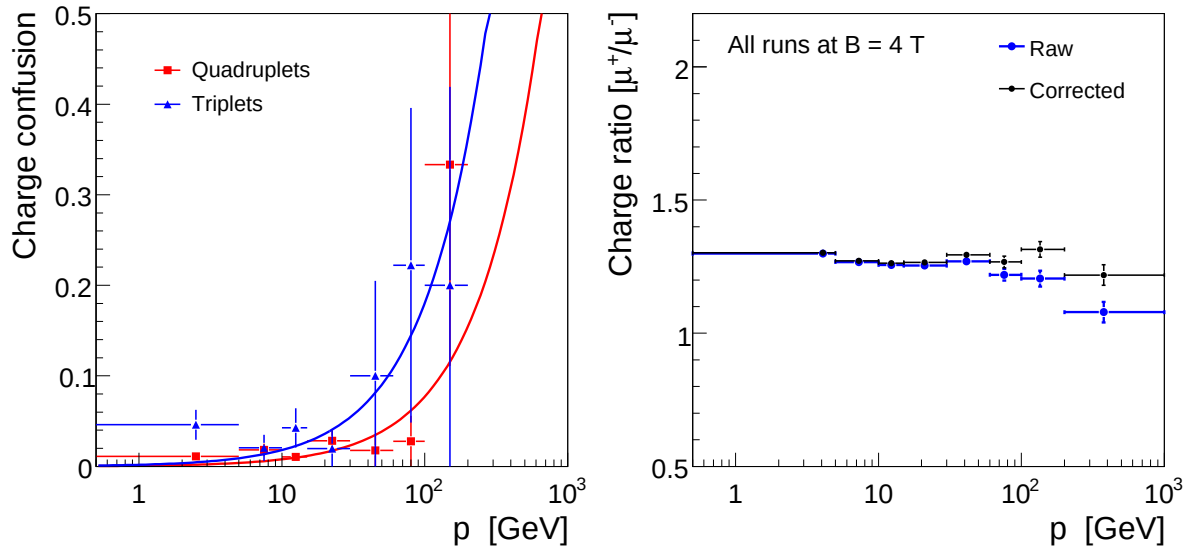

Figure 11: (Left) Charge confusion for quadruplets (red) and triplets (blue), calculated using simulated events. The solid lines represent a linear fit to the dots, constrained to be zero at $p = 0$. (Right) Effect of applying the correction due to charge confusion to the measured charge ratio, for the combined result. The error bars indicate the statistical errors in both cases.

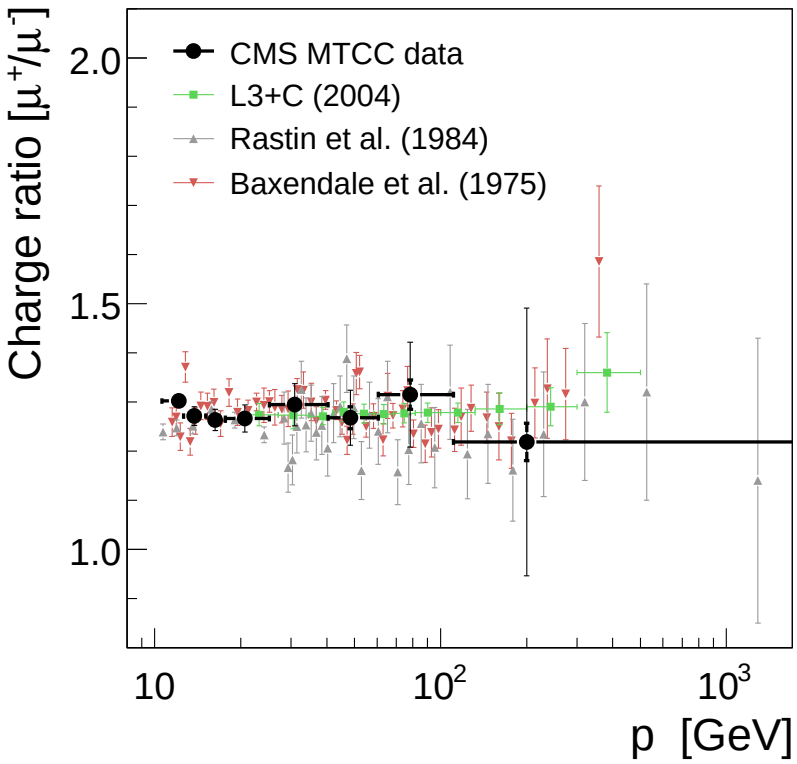

Figure 12: Muon charge ratio measured by CMS (black dots) with statistical (thick bars) and systematic errors (thin bars), together with results from other experiments (other colors).